Direct Observation of Topology from Single-Photon Dynamics

Yao Wang,[1,2] Yong-Heng Lu,[1,3] Feng Mei,[4,5,*] Jun Gao,[1,2] Zhan-Ming Li,[1,3] Hao Tang,[1,3] Shi-Liang Zhu,[6,3] Suotang Jia,[4,5] and Xian-Min Jin[1,3,†]

[1]*School of Physics and Astronomy, Shanghai Jiao Tong University, Shanghai 200240, China*
[2]*Institute for Quantum Science and Engineering and Department of Physics, Southern University of Science and Technology, Shenzhen 518055, China*
[3]*Synergetic Innovation Center of Quantum Information and Quantum Physics, University of Science and Technology of China, Hefei, Anhui 230026, China*
[4]*State Key Laboratory of Quantum Optics and Quantum Optics Devices, Institute of Laser Spectroscopy, Shanxi University, Taiyuan, Shanxi 030006, China*
[5]*Collaborative Innovation Center of Extreme Optics, Shanxi University, Taiyuan, Shanxi 030006, China*
[6]*National Laboratory of Solid State Microstructures and School of Physics, Nanjing University, Nanjing 210093, China*

(Received 11 December 2018; published 16 May 2019)

Topology manifesting in many branches of physics deepens our understanding on state of matters. Topological photonics has recently become a rapidly growing field since artificial photonic structures can be well designed and constructed to support topological states, especially a promising large-scale implementation of these states using photonic chips. Meanwhile, due to the inapplicability of Hall conductance to photons, it is still an elusive problem to directly measure the integer topological invariants and topological phase transitions in photonic system. Here, we present a direct observation of topological winding numbers by using bulk-state photon dynamics on a chip. Furthermore, we for the first time experimentally observe the topological phase transition points via single-photon dynamics. The integrated topological structures, direct measurement in the single-photon regime and strong robustness against disorder add the key elements into the toolbox of "quantum topological photonics" and may enable topologically protected quantum information processing in large scale.

DOI: 10.1103/PhysRevLett.122.193903

The introduction of topology into condensed-matter and material sciences originates from the connection of integer quantum Hall conductances with topological Chern invariants [1], which greatly expands our knowledge on state of matters. With the birth of topological insulators, searching topological state of matters in solid state materials [2,3] and photonic systems [4,5] has recently become a leading research field. In contrast to the challenging experimental requirements for realizing topological states in solid state materials, photonic systems provide a convenient and versatile platform to design various topological lattice models and study different topological states, including topological insulator states [6–10] and topological Weyl points [11,12]. The found topological edge states and phase transition potentially can be utilized for developing inherently robust and efficient artificial photonic devices [13–20].

Although photonic topological edge states have been extensively studied, the photonic topological invariant defined on the bulk states, which is the seminal observable for characterizing topological states, is still less explored. In fermion systems, the topological invariant can be revealed by conductance measurements, while the concept of Hall conductance is inapplicable in photonic systems. Several methods recently have been proposed for indirectly detecting topological invariants, based on probing Berry curvature [21,22], non-Hermitian photon loss [23,24], bulk-edge correspondence [25,26], and phase spectroscopy [27]. Nevertheless, direct measuring photonic topological invariants remains elusive.

Waveguide lattice provides a natural platform for studying photon dynamics. The reason is that the propagation of photons in a photonic waveguide lattice is naturally equivalent to a time evolution. However, direct measuring topological invariants based on photon dynamics has never been reported before in topological waveguide lattices. Here, for the first time, we experimentally demonstrate that both the topological invariants and the topological phase transitions can be directly measured based on the propagation of photons in the bulk of a topological waveguide lattice. Our work generalizes the method proposed in linear optics–based quantum walks [28,29] to use continue-time dynamics to directly measure topology. This dynamical method is very generic for observing topology, which recently also has been experimentally demonstrated in ultracold atoms [30].

To extend promised topological protection into the quantum regime, we have to find an appropriate system that is physically scalable and has inherently low loss when

 © 2019 American Physical Society

scaling up. Integrated photonics can meet the first requirement elegantly by constructing topological waveguide lattice on a photonic chip in a physically scalable fashion [31,32], with which topological states can be generated, manipulated, and detected in a very high complexity beyond that conventional bulk optics can do [28,29]. Meanwhile, realizing topological states in Hermitian systems can well meet the second requirement since the intrinsic loss in non-Hermitian systems [24] will induce an evolution of exponential decay for single photons and multiplicative inefficiency for multi-photons.

Here, we integrate topological waveguide lattices on a photonic chip and experimentally demonstrate a direct observation of the topological invariants in the constructed Hermitian system using bulk-state photon dynamics. Through initially injecting photons into the middle waveguide to excite the bulk state, the values of topological winding numbers can be extracted from the chiral photonic density centers associated with the final output distribution. We further extend the topological system and measurement into quantum regime by observing the topological phase transition point via single-photon dynamics. With the bulk state excited by heralded single photons, we can successfully identify the topological phase transition point separating the topological trivial and nontrivial phases, even with artificially introduced disorder.

Topological photonic lattice.—As is shown in Fig. 1(a), we fabricate waveguide lattices in borosilicate glass by using the femtosecond laser direct writing technique [31–37] (see the Supplemental Material, part A [38] for the fabrication and measurement of the integrated topological photonic lattices). The constructed lattices are based on the Su-Schrieffer-Heeger model, which describes a one-dimensional lattice with alternating strong and weak couplings. The Hamiltonian of this model could be written as [39,40]

$$\mathrm{H} = \sum_{x} (J_1 a_x^{+} b_x + J_2 b_x^{+} a_{x+1}) + \mathrm{H.c.}, \tag{1}$$

where each unit cell in the chain consists of two sites labeled as a and b; the terms $a_x^{+}(a_x)$ and $b_x^{+}(b_x)$ are the creation (annihilation) operators for the two sites in the x unit cell, and the coefficients J_1 and J_2 represent the intracell and intercell coupling strengths, respectively. In the waveguide lattice, the site is represented by the waveguide and the longitudinal direction of lattice maps the evolution time. To study the topological feature, we rewrite Eq. (1) in momentum space as $\hat{H} = \sum_{k_x} \hat{h}(k_x)$, where $\hat{h}(k_x) = d_x \hat{\tau}_x + d_y \hat{\tau}_y$, $d_x = J_1 + J_2 \cos(k_x)$, $d_y = J_2 \sin(k_x)$, and $\hat{\tau}_x$ and $\hat{\tau}_y$ are the Pauli spin operators defined in the momentum space. The energy bands of the Hamiltonian are characterized by the topological winding number

$$\nu = \frac{1}{2\pi} \int dk_x \mathbf{n} \times \partial_{k_x} \mathbf{n}, \tag{2}$$

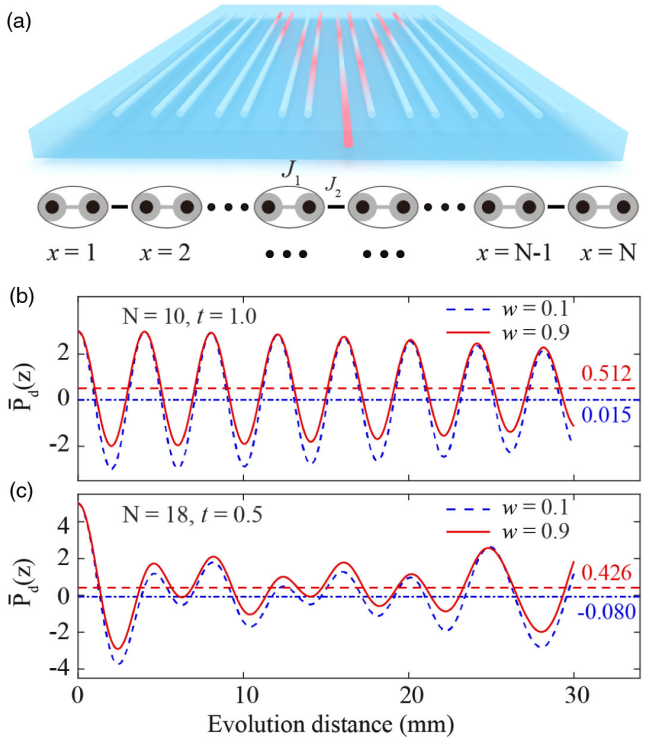

FIG. 1. Schematic of the integrated topological photonic lattice, model, and simulation. (a) Sketch of Su-Schrieffer-Heeger model. The unit cell label x is marked starting from the edge of the system with 1. Every unit cell consists of two sites and every site is implemented by a laser-written waveguide. (b),(c) Simulated results. The values of PPDC oscillate around 0 and 0.5 for $w = 0.1$ and $w = 0.9$ corresponding to the systems in topological trivial and nontrivial phases, respectively. The numbers on the right side of the figure present the averaged values of PPDC. The value of g is set to 0.5.

where $\mathbf{n} = (n_x, n_y) = (d_x, d_y)/\sqrt{d_x^2 + d_y^2}$. We manipulate the coupling coefficients as $J_1 = g + gt\cos(w\pi)$ and $J_2 = g - gt\cos(w\pi)$, where $g > 0$, $0 < w < 1$, and $0 \le t \le 1$. The system is in the topological nontrivial phase with the winding number $\nu = 1$ when $J_1 < J_2$, i.e., $w \in (0.5, 1)$. Otherwise, it is in the topological trivial phase with $\nu = 0$ when $J_1 > J_2$, i.e., $w \in (0, 0.5)$. The topological phase transition point appears when $J_1 = J_2$ (see the Supplemental Material, part B [38] for the topology of the integrated photonic lattices).

Dynamical detection of topological winding number.—To detect the winding number of the lattice on the topological photonic chip, we introduce a photon population difference center (PPDC) $P_d = \sum_x x(a_x^{+} a_x - b_x^{+} b_x)$, where the unit cell index x is shown in Fig. 1(a). We inject photons into the middle waveguide to excite the bulk state. With the evolution of the photons over a distance z in the lattice, the corresponding PPDC can be denoted as $\bar{P}_d(z)$. We find that the topological winding number ν can be measured via the evolution distance–averaged PPDC $\bar{P}_d(z)$, which can be expressed as

$$\nu = 2\lim_{Z\to\infty}\frac{1}{Z}\int_0^Z dz\bar{P}_d(z), \tag{3}$$

where z is the evolution distance (see the Supplemental Material, part C [38] for the relationship between topological winding number and PPDC). In Figs. 1(b) and 1(c), we calculate the $\bar{P}_d$ for different coupling coefficients and lattice sizes. The results show that the values of PPDC $\bar{P}_d$ keep oscillating centered at 0 and 0.5 when the lattice is in the topological trivial and nontrivial phases, respectively. The topological winding numbers derived as $\nu = 0$ and $\nu = 1$ can be directly measured from the output density distribution.

In the experiment, we implement a topological photonic lattice consisting of 10 waveguides with $t = 1.0$. To perform the evolution-distance average, we integrate 40 such photonic lattices on a single chip with different evolution distances varying from 20 to 30 mm with a step size of 0.2 mm. We excite one waveguide in the central unit cell ($x = 3$) with a narrow-band coherent light at 852 nm, and measure the output density from each photonic lattice. The evolution distance–dependent PPDC is extracted and shown in Figs. 2(a) and 2(b). The result in Fig. 2(a) shows that, when the system is in the topological trivial phase, the values of PPDC $\bar{P}_d$ keep oscillating centered at 0.045 ± 0.090. While the system is in the topological nontrivial phase, $\bar{P}_d$ keeps oscillating around 0.540 ± 0.070 as shown in Fig. 2(b). According to Eq. (3), we obtain the topological winding numbers $\nu = 0.09 \pm 0.18$ and $\nu = 1.08 \pm 0.14$ for the two phases, respectively. We can see that the oscillation of the measured P_d values is more irregular than that of the simulated result, but the winding number can still be clearly extracted.

To further experimentally demonstrate the reliability and universality of our approach, we fabricate another set of photonic lattices consisting of 18 waveguides with $t = 0.5$. The evolution distance varies from 7 to 16 mm with a step size of 0.2 mm. As is shown in Figs. 2(c) and 2(d), when the lattices are prepared in the topological trivial and nontrivial phases, the measured values of $\bar{P}_d$ are oscillating around 0.095 ± 0.16 and 0.526 ± 0.014, which lead to the topological winding numbers of $\nu = 0.19 \pm 0.32$ and $\nu = 1.052 \pm 0.28$, respectively. The experimental results are well consist with the simulated results shown in Fig. 1(c) and suggest that our proposed dynamical approach of measuring topological invariants is insensitive to the detailed lattice configurations. See Supplemental Material, part D [38] for the influence of photon losses and noise on PPDC, which includes Ref. [41].

Dynamical detection of topological phase transition.—We have shown that the topological winding numbers associated with bulk-state photon dynamics can be directly observed by imaging the output density distribution of light. In the following, by developing heralded single-photon source and single-photon imaging technique, we are able to push our approach into quantum regime and

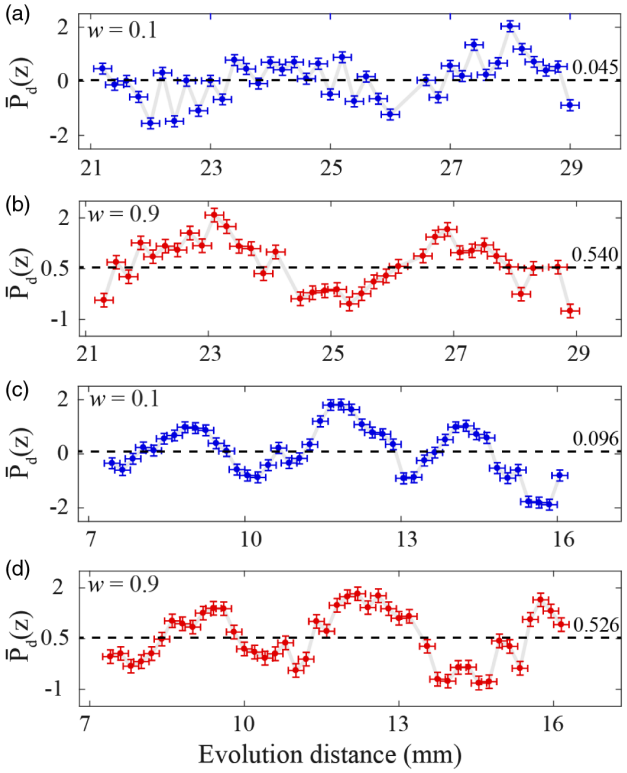

FIG. 2. Experimental results of PPDC. The measured values of PPDC for 10-sited (a),(b) and 18-sited (c),(d) lattices, which are found oscillating around 0 (a),(c) and 0.5 (b),(d) for the systems in topological trivial and nontrivial phases. The averaged values of PPDC $\bar{P}_d$ are 0.045 ± 0.090 (a) and 0.540 ± 0.070 (b) for the case of $t = 1.0$, and are 0.095 ± 0.16 (c) and 0.526 ± 0.014 (d) for the case of $t = 0.5$, respectively.

demonstrate the direct observation of the topological phase transition via single-photon dynamics.

The transition point of band structure of the photonic lattice can be revealed by the generalized photon population center $P_c = \sum_x x^2(a_x^+ a_x + b_x^+ b_x)$, where the label x is marked as shown in Fig. 3(a) for a concise expression. With the bulk state excited from the central unit cell by single photons, the value of generalized photon population center can be derived as $\bar{P}_c(z)$ for an evolution distance z. We can further obtain the topological phase transition signal (TPTS) $S_t = \bar{P}_c(z)/z^2$, and we find that (see the Supplemental Material, part E [38] for the relationship between TPTS and photon population center)

$$S_t = \begin{cases} \frac{J_1^2}{2}, & J_1 < J_2 \\ \frac{J_2^2}{2}. & J_1 > J_2 \end{cases}. \tag{4}$$

The simulated results are illustrated in Fig. 3(b). For a continuously transitive system from topological nontrivial to trivial, as is sketched with the red points, the TPTS value increases firstly and then decreases, and the maximum value arises when the system undergoes the topological

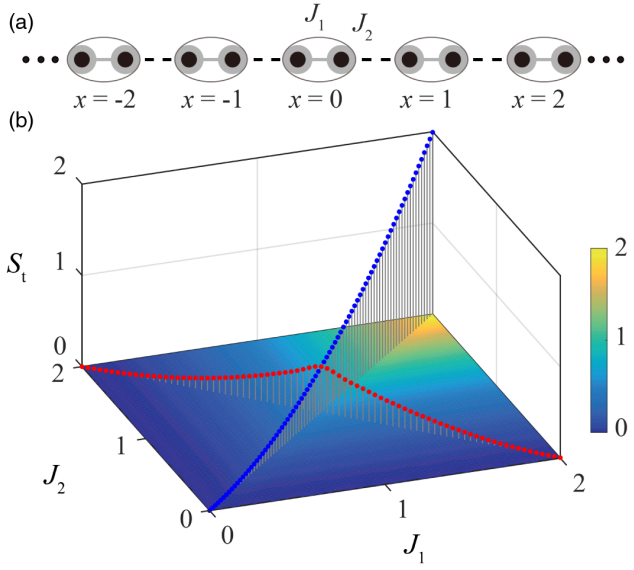

FIG. 3. Theoretical results of TPTS. (a) The Su-Schrieffer-Heeger model with the labels marked starting from middle of the system for a concise expression of the photon population center. (b) The simulated results of TPTS. The dynamical TPTS value increases and then decreases for a continuous transitive system (red point), and the transition point will be more distinct in the strong interaction region (blue point).

phase transition point. Unlike the statistical measurement of PPDC, this approach requires only single measurement on generalized photon population center for a certain structure; the topological transition point therefore can be more conveniently observed in experiment. When the dynamical TPTS value varies with the increasing of the value of J_1 and J_2, the transition points as sketched with blue points will be more distinct to be observed in the strong interaction region.

To experimentally observe the TPTS in a continuous transitive system, we fabricate 11 set of photonic lattices with lattice constant $d = 20$ μm and different intracell (d_1) and intercell (d_2) space. The dimerization $\Delta d = (d_2 - d_1)/2$ varies from -2 to 2 μm in a step of 0.5 μm for nine lattices, and two more lattices are designed near the transition point with the dimerization values of -0.2 and 0.2 μm. The coupling strength is modulated by the separation between adjacent waveguides, which is not linear according to coupling mode theory [see Fig. 4(a)]. The corresponding coupling strength of J_1 and J_2 defined by the dimerization values in 11 lattices are marked with red squares in Fig. 4(b). All the lattices consist of 42 sites (21 untie cells) and have an evolution distance of 18 mm to ensure that the photons will not evolve to the edge. We prepare heralded single photons at 810 nm via spontaneous parametric down-conversion (see the Supplemental Material, part F [38] for the generation and imaging of the heralded single photons) and excite the bulk state from one of two sites in the central unit cell ($x = 0$).

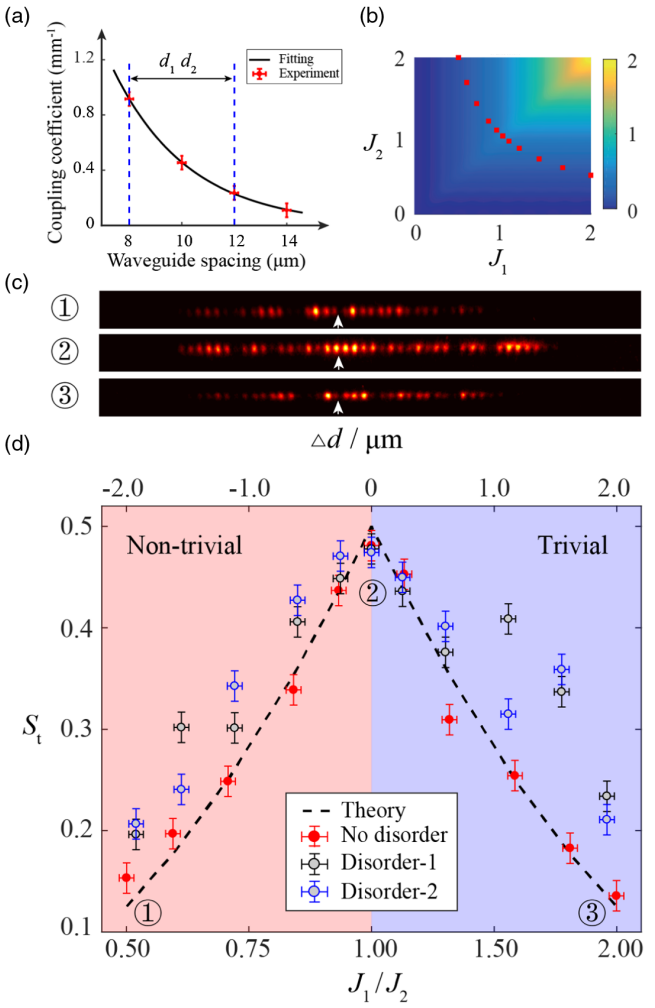

FIG. 4. Experimental results of TPTS. (a) The relation between the coupling strength and the separation between adjacent waveguides. The blue dash lines mark the experimentally accessible range of d_1 and d_2. (b) The coupling strength of J_1 and J_2 of the 11 lattices used in experiment (red squares). (c) The evolution probability distribution of single photons in topological nontrivial phase, transition point, and trivial phase. The blank arrows mark the excited sites in experiment. (d) The measured results of TPTS. The topological transition point appears when the system undergoes the phase transition from the topological nontrivial to trivial phase (red circles), even with artificially introduced disorder (black and blue circles). Error derivation can be found in the Supplemental Material, part G [38].

We show the experimental results in Figs. 4(c) and 4(d). Directly from the evolution probability distribution of single photons, we cannot find distinct criteria to distinguish when the lattice is in topological nontrivial phase, transition point, and trivial phase [see Fig. 4(c)]. In Fig. 4(d), we plot the experimental (red dots) and theoretical (black dash line) results of TPTS S_t varying with the coupling strength ratio J_1/J_2 (and dimerization Δd). The values of S_t increase with the square of J_1 when $J_1/J_2 < 1$ and decrease

with the square of J_2 when $J_1/J_2 > 1$. As a result, the signal of the topological transition point appears very clearly when the $J_1/J_2 = 1$, corresponding to the $\Delta d = 0$.

Besides the advantage of directly observing topological transition point, it would be also interesting to test the robustness of this approach. We manage to introduce the disorder into the system by adding random fluctuation of ± 0.1 μm to d_1 and d_2 in the laser writing process. We fabricate 11 set of such disorder-embedded lattices and repeat the experiment twice. As is shown in Fig. 4(c), the experimental results retrieved from the 22 lattices indicate that while the measured values of S_t randomly deviate from the theoretical curve assumed for the ideal case, the topological transition point still can be clearly identified around $J_1/J_2 = 1$.

In summary, we have experimentally demonstrated direct observation of the photonic topological invariants and topological phase transition through the photon dynamics in the bulk state of topological waveguide lattice. This approach based on single-particle dynamics in the real space provides a new route for direct measurement of topology [28–30], which complements the approach in ultracold atomic systems using Bloch state dynamics in the momentum space [42,43].

Direct observation of topology in higher-dimensional system via single-photon dynamics is of great interest and is more experimentally challenging. It is possible to generalize our approach to detect the topological phase transition in two-dimensional lattices such as photonic graphene, since the photonic dynamics in the gapless phase is distinctly different from the one in the gapped phase. For example, the topological transition point can be clearly manifested by measuring TPTS in two-dimensional lattices.

The demonstrated key elements, including integrated topological structures, direct measurement in single-photon regime and strong robustness against disorder, can enrich the emerging field of "quantum topological photonics." With the primary attempt to combine topology with quantum integrated photonics [31,32,44], it is promising to explore scalable topologically protected quantum information processing on topological photonic chips beyond classical topological photonics. The prompt questions, but remain open, will be whether we can directly observe topology with multiphoton dynamics and how qubit and entanglement behave.

The authors thank Ian Walmsley and Jian-Wei Pan for helpful discussion. This research is supported by the National Key R&D Program of China (Grants No. 2017YFA0303700, No. 2017YFA0304203, and No. 2016YFA0301803), National Natural Science Foundation of China (Grants No. 61734005, No. 11761141014, No. 11690033, and No. 11604392), Science and Technology Commission of Shanghai Municipality (Grants No. 16JC1400405 and No. 17JC1400403), Shanghai Municipal Education Commission (Grants No. 16SG09 and No. 2017-01-07-00-02-E00049), Program for Changjiang Scholars and Innovative Research Team in University (Grant No. IRT 17R70), and the Shanxi 1331KSC and 111 Project (Grant No. D18001). X.-M. J. acknowledges support from the National Young 1000 Talents Plan.

*meifeng@sxu.edu.cn
†xianmin.jin@sjtu.edu.cn

[1] D. J. Thouless, M. Kohmoto, M. P. Nightingale, and M. den Nijs, Quantized Hall Conductance in a Two-Dimensional Periodic Potential, Phys. Rev. Lett. **49**, 405 (1982).
[2] M. Z. Hasan and C. L. Kane, Colloquium: Topological insulators, Rev. Mod. Phys. **82**, 3045 (2010).
[3] X.-L. Qi and S.-C. Zhang, Topological insulators and superconductors, Rev. Mod. Phys. **83**, 1057 (2011).
[4] L. Lu, J. D. Joannopoulos, and M. Soljačić, Topological photonics, Nat. Photonics **8**, 821 (2014).
[5] T. Ozawa *et al.*, Topological photonics, Rev. Mod. Phys. **91**, 015006 (2019).
[6] F. D. M. Haldane and S. Raghu, Possible Realization of Directional Optical Waveguides in Photonic Crystals with Broken Time-Reversal Symmetry, Phys. Rev. Lett. **100**, 013904 (2008).
[7] Z. Wang, Y. Chong, J. D. Joannopoulos, and M. Soljačić, Observation of unidirectional backscattering-immune topological electromagnetic states, Nature (London) **461**, 772 (2009).
[8] M. Hafezi, E. A. Demler, M. D. Lukin, and J. M. Taylor, Robust optical delay lines with topological protection, Nat. Phys. **7**, 907 (2011).
[9] A. B. Khanikaev, S. H. Mousavi, W.-K. Tse, M. Kargarian, A. H. MacDonald, and G. Shvets, Photonic topological insulators, Nat. Mater. **12**, 233 (2013).
[10] M. C. Rechtsman, J. M. Zeuner, Y. Plotnik, Y. Lumer, D. Podolsky, F. Dreisow, S. Nolte, M. Segev, and A. Szameit, Photonic Floquet topological insulators, Nature (London) **496**, 196 (2013).
[11] L. Lu, Z. Wang, D. Ye, L. Ran, L. Fu, J. D. Joannopoulos, and M. Soljačić, Experimental observation of Weyl points, Science **349**, 622 (2015).
[12] J. Noh, S. Huang, D. Leykam, Y. D. Chong, K. P. Chen, and M. C. Rechtsman, Experimental observation of optical Weyl points and Fermi arcs, Nat. Phys. **13**, 611 (2017).
[13] N. Malkova, I. Hromada, X. Wang, G. Bryant, and Z. Chen, Observation of optical Shockley-like surface states in photonic superlattices, Opt. Lett. **34**, 1633 (2009).
[14] T. Kitagawa, M. S. Rudner, E. Berg, and E. Demler, Exploring topological phases with quantum walks, Phys. Rev. A **82**, 033429 (2010).
[15] T. Kitagawa, M. A. Broome, A. Fedrizzi, M. S. Rudner, E. Berg, I. Kassal, A. Aspuru-Guzik, E. Demler, and A. G. White, Observation of topologically protected bound states in photonic quantum walks, Nat. Commun. **3**, 882 (2012).
[16] M. C. Rechtsman, Y. Plotnik, J. M. Zeuner, D. Song, Z. Chen, A. Szameit, and M. Segev, Topological Creation and Destruction of Edge States in Photonic Graphene, Phys. Rev. Lett. **111**, 103901 (2013).

[17] M. Hafezi, S. Mittal, J. Fan, A. Migdall, and J. M. Taylor, Imaging topological edge states in silicon photonics, Nat. Photonics **7**, 1001 (2013).
[18] Y. E. Kraus, Y. Lahini, Z. Ringel, M. Verbin, and O. Zilberberg, Topological States and Adiabatic Pumping in Quasicrystals, Phys. Rev. Lett. **109**, 106402 (2012).
[19] V. D. Lago, M. Atala, and L. E. F. F. Torres, Floquet topological transitions in a driven one-dimensional topological insulator, Phys. Rev. A **92**, 023624 (2015).
[20] A. Blanco-Redondo, I. Andonegui, M. J. Collins, G. Harari, Y. Lumer, M. C. Rechtsman, B. J. Eggleton, and M. Segev, Topological Optical Waveguiding in Silicon and the Transition between Topological and Trivial Defect States, Phys. Rev. Lett. **116**, 163901 (2016).
[21] T. Ozawa and I. Carusotto, Anomalous and Quantum Hall Effects in Lossy Photonic Lattices, Phys. Rev. Lett. **112**, 133902 (2014).
[22] M. Wimmer, H. M. Price, I. Carusotto, and U. Peschel, Experimental measurement of the Berry curvature from anomalous transport, Nat. Phys. **13**, 545 (2017).
[23] M. S. Rudner and L. S. Levitov, Topological Transition in a Non-Hermitian Quantum Walk, Phys. Rev. Lett. **102**, 065703 (2009).
[24] J. M. Zeuner, M. C. Rechtsman, Y. Plotnik, Y. Lumer, S. Nolte, M. S. Rudner, M. Segev, and A. Szameit, Observation of a Topological Transition in the Bulk of a Non-Hermitian System, Phys. Rev. Lett. **115**, 040402 (2015).
[25] M. Hafezi, Measuring Topological Invariants in Photonic Systems, Phys. Rev. Lett. **112**, 210405 (2014).
[26] S. Mittal, S. Ganeshan, J. Fan, A. Vaezi, and M. Hafezi, Measurement of topological invariants in a 2D photonic system, Nat. Photonics **10**, 180 (2016).
[27] A. V. Poshakinskiy, A. N. Poddubny, and M. Hafezi, Phase spectroscopy of topological invariants in photonic crystals, Phys. Rev. A **91**, 043830 (2015).
[28] F. Cardano, M. Maffei, F. Massa, B. Piccirillo, C. de Lisio, G. De Filippis, V. Cataudella, E. Santamato, and L. Marrucci, Statistical moments of quantum-walk dynamics reveal topological quantum transitions, Nat. Commun. **7**, 11439 (2016).
[29] F. Cardano *et al.*, Detection of Zak phases and topological invariants in a chiral quantum walk of twisted photons, Nat. Commun. **8**, 15516 (2017).
[30] E. J. Meier, F. Alex An, A. Dauphin, M. Maffei, P. Massignan, T. L. Hughes, and B. Gadway, Observation of the topological Anderson insulator in disordered atomic wires, Science **362**, 929 (2018).
[31] H. Tang *et al.*, Experimental two-dimensional quantum walk on a photonic chip, Sci. Adv. **4**, eaat3174 (2018).
[32] H. Tang *et al.*, Experimental quantum fast hitting on hexagonal graphs, Nat. Photonics **12**, 754 (2018).
[33] K. M. Davis, K. Miura, N. Sugimoto, and K. Hirao, Writing waveguides in glass with a femtosecond laser, Opt. Lett. **21**, 1729 (1996).
[34] A. Szameit, F. Dreisow, T. Pertsch, S. Nolte, and A. Tünnermann, Control of directional evanescent coupling in fs laser written waveguides, Opt. Express **15**, 1579 (2007).
[35] A. Crespi, R. Osellame, R. Ramponi, D. J. Brod, E. F. Galvão, N. Spagnolo, C. Vitelli, E. Maiorino, P. Mataloni, and F. Sciarrino, Integrated multimode interferometers with arbitrary designs for photonic boson sampling, Nat. Photonics **7**, 545 (2013).
[36] Z. Chaboyer, T. Meany, L. G. Helt, M. J. Withford, and M. J. Steel, Tunable quantum interference in a 3D integrated circuit, Sci. Rep. **5**, 9601 (2015).
[37] Y. Wang *et al.*, Parity-Induced Thermalization Gap in Disordered Ring Lattices, Phys. Rev. Lett. **122**, 013903 (2019).
[38] See Supplemental Material at http://link.aps.org/supplemental/10.1103/PhysRevLett.122.193903 for more details.
[39] W. P. Su, J. R. Schieffer, and A. J. Heeger, Solitons in Polyacetylene, Phys. Rev. Lett. **42**, 1698 (1979).
[40] D. W. Zhang, Y. Q. Zhu, Y. X. Zhao, H. Yan, and S. L. Zhu, Topological quantum matter with cold atoms, Adv. Phys. **67**, 253 (2018).
[41] M. Golshani, S. Weimann, Kh. Jafari, M. Khazaei Nezhad, A. Langari, A. R. Bahrampour, T. Eichelkraut, S. M. Mahdavi, and A. Szameit, Impact of Loss on the Wave Dynamics in Photonic Waveguide Lattices, Phys. Rev. Lett. **113**, 123903 (2014).
[42] M. Atala, M. Aidelsburger, J. T. Barreiro, D. Abanin, T. Kitagawa, E. Demler, and I. Bloch, Direct measurement of the Zak phase in topological Bloch bands, Nat. Phys. **9**, 795 (2013).
[43] N. Fläschner, B. S. Rem, M. Tarnowski, D. Vogel, D.-S. Luhmann, K. Sengstock, and C. Weitenberg, Experimental reconstruction of the Berry curvature in a Floquet Bloch band, Science **352**, 1091 (2016).
[44] J. L. Tambasco, G. Corrielli, R. J. Chapman, A. Crespi, O. Zilberberg, R. Osellame, and A. Peruzzo, Quantum interference of topological states of light, Sci. Adv. **4**, eaat3187 (2018).